Investigation of the Dinuclear Fe Center of Methane Monooxygenase by Advanced Paramagnetic Resonance Techniques: On the Geometry of DMSO Binding

Victoria J. DeRose,[†] Katherine E. Liu,[‡] Stephen J. Lippard,*[,‡] and Brian M. Hoffman*[,†]

Contribution from the Departments of Chemistry, Northwestern University, Evanston, Illinois 60208, and Massachusetts Institute of Technology, Cambridge, Massachusetts 02139

Received April 5, 1995[⊗]

Abstract: We report an extensive advanced paramagnetic resonance characterization of the mixed-valence dinuclear Fe center of methane monooxygenase hydroxylase ($MMOH_{mv}$) from *Methylococcus capsulatus (Mc)* (Bath) and of binding to it by the exogenous ligand DMSO. We employ continuous wave and pulsed electron nuclear double resonance (ENDOR) spectroscopy, both at Q-band microwave frequencies, to examine $^{14,15}N$, $^{1,2}H$, ^{13}C, and ^{57}Fe nuclei. Preliminary ^{1}H ENDOR results were communicated previously (DeRose, V. J.; Liu, K. E.; Hoffman, B. M.; Lippard, S. J. *J. Am. Chem. Soc.* **1993**, *115*, 6440−6441). ENDOR-derived $^{14,15}N$ hyperfine tensors are interpreted in terms of the spin distribution on histidyl ligands bound to the dinuclear center. Determination of the ^{57}Fe hyperfine tensors gives a complete picture of the spin-coupled Fe^{2+} and Fe^{3+} ions. The $^{1,2}H$ ENDOR results disclose the presence of a bridging hydroxide and an aqua ligand in both native and DMSO-treated enzyme. A novel procedure for describing the ^{1}H hyperfine tensor of the bridge gives the orientation of the **g**-tensor relative to the cluster framework in both enzyme forms, information that is normally obtained only from full single-crystal EPR studies. DMSO is found to cause small perturbations of both histidyl ligands, and little change in the ^{57}Fe hyperfine tensors. However, Q-band pulsed ^{2}H and ^{13}C ENDOR measurements of labeled DMSO show that this exogenous ligand binds in a distinct site with a well-ordered structure, and further indicate that it is O-bound to the Fe^{3+} ion of the mixed-valence cluster. The analysis, coupled with ^{2}H X-band electron spin−echo envelope modulation data, places limitations on the possible orientation of the bound DMSO. These geometric restrictions have been used to guide molecular modeling of DMSO bound to the $MMOH_{mv}$ diiron active site. The results reported here provide a basis with which to study other dinuclear Fe−carboxylate proteins.

Introduction

Methane monooxygenase (MMO) catalyzes the dioxygen-dependent oxidation of methane to yield methanol (eq 1) in the first step of the carbon utilization pathway in methanotrophic organisms. Both Fe-containing soluble and Cu-containing

$$CH_4 + O_2 + 2e^- + 2H^+ \rightarrow CH_3OH + H_2O \qquad (1)$$

membrane-bound MMO proteins are known, with only the Fe form being expressed under conditions of low Cu concentrations. The soluble forms of MMO from the methanotrophs *Methylococcus capsulatus (*Bath) (*Mc*)[1] and *Methylosinus trichosporium* OB3b (*Mt*)[2] have been the most extensively studied. The MMO complex consists of three components: a Fe_2 hydroxylase (MMOH, 251 kD), a Fe_2S_2-flavin reductase (MMOR, 38.6 kD), and a regulatory protein (component B, 15.5 kD). Reaction 1 is catalyzed by the dinuclear Fe center of MMOH, with reducing equivalents being provided by MMOR. Component B appears to couple binding and reactivity of both reductase and substrate to MMOH.[3,4] In addition to its natural substrate, MMOH catalyzes the oxidation of a variety of xenobiotic species;[5] the potential for its use in bioremediation of environmental hazards along with its unique ability to activate methane have further stimulated structural and mechanistic studies of the hydroxylase.

Biophysical characterization of the dinuclear Fe center of MMOH places it within an emerging class of carboxylate bridged diiron enzymes with diverse and unusual reactivities; these include hemerythrin, ribonucleotide reductase, and uteroferrin.[6−8] The X-ray structures of several of these are known, providing a foundation from which to pose mechanistic questions. The structure of MMOH from *M. capsulatus* in the oxidized, diferric form ($MMOH_{ox}$) has been recently determined by X-ray crystallography to 2.2 Å at 4 °C and to 1.7 Å in frozen crystals.[9,10] Each α subunit of the $\alpha_2\beta_2\gamma_2$ hexamer contains one diiron site, the local structure of which is shown in Figure 1. The terminal ligand environment of the Fe center includes a single histidine per Fe, several protein-derived carboxylate ligands, and a terminal aqua ligand. A hydroxide ion, a glutamate carboxylate, and an acetate (from the crystallizing buffer at 4 °C) or water molecule (frozen crystals) form bridging

[†] Northwestern University.
[‡] Massachusetts Institute of Technology.
[⊗] Abstract published in *Advance ACS Abstracts,* December 15, 1995.

(1) Liu, K. E.; Lippard, S. J. In *Advances in Inorganic Chemistry*; Sykes, G., Ed.; 1995; Vol. 42, pp 263−289.
(2) Lipscomb, J. D. *Annu. Rev. Microbiol.* **1994**, *48*, 371−399.
(3) Liu, K. E.; Lippard, S. J. *J. Biol. Chem.* **1991**, *266*, 12836−12839, 24859.
(4) Green, J.; Dalton, H. *Biochem. J.* **1989**, *259*, 167−172.
(5) Green, J.; Dalton, H. *J. Biol. Chem.* **1989**, *264*, 7698−7703.
(6) Lippard, S. J. *Angew. Chem., Int. Ed. Engl.* **1988**, *27*, 344−361.
(7) Que, L., Jr.; True, A. E. In *Progress in Inorganic Chemistry*; Lippard, S. J., Ed.; J. Wiley & Sons: New York, 1990; Vol. 38, pp 97−200.
(8) Vincent, J. B.; Olivier-Lilley, G. L.; Averill, B. A. *Chem. Rev.* **1990**, *90*, 1447−1467.
(9) Rosenzweig, A. C.; Frederick, C. A.; Lippard, S. J.; Nordlund, P. *Nature* **1993**, *366*, 537−543.
(10) Rosenzweig, A. C.; Nordlund, P.; Takahara, P. M.; Frederick, C. A.; Lippard, S. J. *Chem. Biol.* **1995**, *2*, 409−418.

0002-7863/96/1518-0121$12.00/0

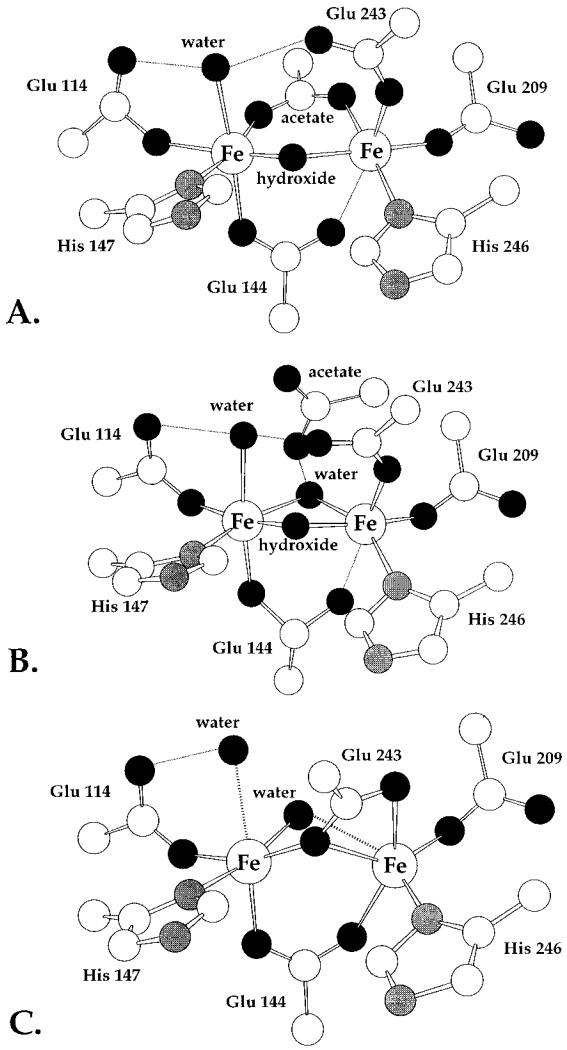

Figure 1. Structure of the oxidized and reduced dinuclear Fe center of MMOH from *M. capsulatus* (Bath) as deduced from X-ray crystallographic studies: (A) $MMOH_{ox}$, collected at 4 °C, 2.2 Å resolution;[9] (B) $MMOH_{ox}$, flash-frozen crystals collected at −140 °C, 1.7 Å A resolution;[10] (C) $MMOH_{red}$, obtained from soaking crystals of $MMOH_{ox}$ in sodium dithionite and methyl viologen, flash-frozen crystals, collected at −140 °C, 1.7 Å resolution.[10] Short dashed lines indicate hydrogen bonds whereas long dashed lines signify little or no interaction (after ref 10).

ligands and complete the coordination sphere of each Fe. In the reduced, diiron(II) form, the hydroxide bridge is extruded by the oxygen atom of Glu 209 which shifts into the bridging position and the water molecules are very weakly bound.[10]

These results indicate that the coordination environment of the diiron center is susceptible to changes induced by carboxylate shifts, which opens the question of how the enzymatic reactivity of the MMOH dinuclear center relates to its structure. For example, proposed mechanisms for methane hydroxylation suggest coordination and activation of dioxygen by the diiron center, and both (μ-peroxo) diiron(III) and diferryl species have been proposed as kinetic intermediates.[1,2] As depicted in Figure 1, the two Fe ions of $MMOH_{ox}$ are coordinatively saturated, but there are available sites for dioxygen binding and μ-peroxo formation in $MMOH_{red}$. These observations pertain to solid state structures, however, and it is important to obtain equivalent information about the solution state.

The EPR spectrum of the mixed-valent form $MMOH_{mv}$ (g_{av} = 1.82), which is characteristic of this class of $Fe^{2+}Fe^{3+}$ centers,[11−15] is sensitive to treatment with exogenous ligands such as dimethyl sulfoxide and the product methanol.[15] The EPR signal further exhibits a large shift in *g*-value and power-saturation characteristics in the presence of MMO protein component B.[14,16] These changes in the EPR signal reflect alterations of the local structure about the Fe atoms, but do not necessarily indicate that small molecules bind to the dinuclear center. The effect of protein B, in particular, must be allosteric in nature since the Fe center is >10 Å from the protein surface. These observations are an extremely valuable complement to crystallographic data since they pertain to the solution state and reveal the effects of protein−protein interactions.

To characterize the flexibility of the coordination environment in the native enzyme, and to provide a spectroscopic basis for addressing mechanistic questions for this and other such dinuclear Fe centers, we have undertaken an extensive characterization of $MMOH_{mv}$ and its DMSO-treated form by multinuclear Q-band CW and pulsed advanced paramagnetic resonance techniques.[17] These techniques, which include electron-nuclear double resonance (ENDOR) and electron spin−echo envelope modulation (ESEEM) spectroscopies, measure the hyperfine interaction between the unpaired electron spin of a center and the surrounding nuclei by means of an EPR-detected nmr signal;[17−20] interpretation of the hyperfine interaction gives both electronic and geometric information about the paramagnetic center.

Previously we used Q-band CW ENDOR to detect a proton assigned to the hydroxide bridge in $MMOH_{mv}$ (*Mc* and *Mt*) and in azidosemimethemerythrin (N_3Hr_{mv}), thus revealing a spectroscopic signature for the {$Fe^{2+}Fe^{3+}$(μ-OH)} moiety.[21] In that work, proton ENDOR resonances were also attributed to a terminal aqua ligand in $MMOH_{mv}$. These results were important in helping to assign electron density for the solvent-derived ligands shown in Figure 1.[9] Other ENDOR and ESEEM studies of $MMOH_{mv}$ have identified signals from the two histidine ligands in both the mixed-valence[15,22] and the direduced[23] forms of the enzyme, which serve as structural probes of perturbations to the cluster. In an X-band ENDOR study of $MMOH_{mv}$ (*Mt*), the resonance assigned as the ^{14}N of histidine ligated to the Fe^{2+} appeared to be greatly altered by treatment with DMSO, leading to the conclusion that DMSO might cause a ligand exchange at Fe^{2+}.[15] Unresolved X-band ENDOR signals from ^2H of deuterated DMSO and methanol also indicated that these

(11) Woodland, M. P.; Patil, D. S.; Cammack, R.; Dalton, H. *Biochim. Biophys. Acta* **1986**, *873*, 237−242.
(12) Prince, R. C.; George, G. N.; Savas, J. C.; Cramer, S. P.; Patel, R. N. *Biochim. Biophys. Acta* **1988**, *952*, 220−229.
(13) Fox, B. G.; Surerus, K. K.; Lipscomb, J. D.; Münck, E. *J. Biol. Chem.* **1988**, *263*, 10553−10556.
(14) DeWitt, J. G.; Bentsen, J. G.; Rosenzweig, A. C.; Hedman, B.; Green, J.; Pilkington, S.; Papaefthymiou, G. C.; Dalton, H.; Hodgson, K. O.; Lippard, S. J. *J. Am. Chem. Soc.* **1991**, *113*, 9219−9235.
(15) Hendrich, M. P.; Fox, B. G.; Andersson, K. K.; Debrunner, P. G.; Lipscomb, J. D. *J. Biol. Chem.* **1992**, *267*, 261−269.
(16) Fox, B. G; Liu, Y.; Dege, J. E.; Lipscomb, J. D. *J. Biol. Chem.* **1991**, *266*, 540−550.
(17) Berliner, L. J.; Reuben, J., Eds. *EMR of Paramagnetic Molecules*; Biological Magnetic Resonance 13; Plenum Press: New York, 1993.
(18) Abragam, A.; Bleaney, B. *Electron Paramagnetic Resonance of Transition Ions*, 2nd ed.; Clarendon Press: Oxford, 1970.
(19) Hoffman, B. M.; DeRose, V. J.; Doan, P. E.; Gurbiel, R. J.; Houseman, A. L. P.; Telser, J. In *EMR of Paramagnetic Molecules*; Biological Magnetic Resonance 13; Berliner, L. J., Reuben, J., Eds.; Plenum Press: New York, 1993; pp 151−218.
(20) DeRose, V. J.; Hoffman, B. M. In *Methods in Enzymology*; Sauer, K., Ed.; Academic Press: New York, 1995; Vol. 23, pp 555−589.
(21) DeRose, V. J.; Liu, K. E.; Kurtz, D. M., Jr.; Hoffman, B. M.; Lippard, S. J. *J. Am. Chem. Soc.* **1993**, *155*, 6440−6441.
(22) Bender, C. J.; Rosenzweig, A. C.; Lippard, S. J.; Peisach, J. *J. Biol. Chem.* **1994**, *269*, 15993−15998.
(23) Hoffman, B. M.; Sturgeon, B. E.; Doan, P. E.; DeRose, V. J.; Liu, K. E.; Lippard, S. J. *J. Am. Chem. Soc.* **1994**, *116*, 6023−6024.

molecules approached the dinuclear center,[15] but the lack of resolution precluded further interpretation of these intriguing results.

The present report addresses the issue of exogenous ligand binding to $MMOH_{mv}$ through a study in which the paramagnetic resonance techniques employed were selected to match the characteristics of the $MMOH_{mv}$ electron-spin system and the particular nucleus being examined.[19,20] Results are reported for $^{1,2}H$, $^{14,15}N$, ^{13}C, and ^{57}Fe sites, with the experimental observations being presented first, followed by analysis. Key features include the following: (i) $^{1,2}H$ ENDOR to probe the influence of DMSO binding on the bridging hydroxide and aqua ligand; (ii) $^{14,15}N$ measurements to resolve the question of how DMSO perturbs the histidyl ligands; (iii) determination of full ^{57}Fe hyperfine tensors to examine ligand-field changes induced by DMSO, thereby complementing and extending the previous Mössbauer study of DMSO-treated MMOH (*Mt*);[24] and (iv) most importantly, Q-band pulsed ^{2}H and ^{13}C ENDOR studies of labeled DMSO coupled with ^{2}H X-band ESEEM data to address the question of whether DMSO binds directly to iron or noncovalently in a hydrophobic pocket as CH_4 might.

Such detailed information about the interaction of a small molecule with the active site serves as a test case for the study of all such diiron proteins. The nature of DMSO binding is of particular mechanistic importance for MMOH because it can delineate potential interaction sites for O_2, substrate, and the product alcohol, all of which are likely to interact with or bind to its diiron center during catalytic turnover.

Methods

Protein Purification and Isotopic Labeling. Growth of native *M. capsulatus* (Bath)[25] and purification of MMOH hydroxylase[14,26] and protein B[26] were carried out as described elsewhere. Specific activities and iron content were in the ranges previously reported.

^{15}N-enriched hydroxylase was isolated from cells grown in medium[25,27] employing KNO_3 (99% ^{15}N, Cambridge Isotope Laboratories). ^{57}Fe-enriched protein samples were obtained by growing cells as described above except that the normal medium was changed such that the source of Fe was $Na^{57}FeEDTA$, prepared in the following manner:[14] ^{57}Fe foil (99%, 7 mg, 0.125 mmole, Cambridge Isotope Labs) was dissolved in 1 mL of ultrapure HNO_3. Next, 0.5 mL of H_2O and 80 mg (0.2 mmol) of $Na_4EDTA{\cdot}2H_2O$ were added. After 5 min of stirring, 4.1 mg (0.1 mmol) of NaOH was added. The resulting mixture was allowed to stir for 6 h, after which it was centrifuged to pellet the precipitate. The dark green supernatant (1 mL) was added to 100 mL of 20 mM sodium phosphate buffer (pH 7.0) and autoclaved as required in preparing the medium for fermentation. A 10 L fermentation was carried out starting from the frozen stocks as described.[27]

Replacement of the exchangeable protons of the hydroxylase by deuterons was achieved in the following manner. Liquid chromatography was carried out at 4 °C at a flow rate of 1 mL/min and with the buffer system 25 mM MOPS (MOPS = *N*-morpholinopropane sulfonic acid) in D_2O, pD 7.0 (as measured with a pH electrode), and 50 mM NaCl unless otherwise specified. Purified hydroxylase (~50 mg) was loaded on a 1.5 × 5 cm Q-Sepharose anion exchange column that was previously equilibrated with 25 mL of buffer. The bound protein was next washed for 30 min and the wash buffer was discarded. Fresh buffer (100 mL) was circulated over the column for 15 h. The hydroxylase was then eluted with buffer containing 0.3 M NaCl.

Preparation of Samples for ENDOR Study. MMOH, ~50 mg per sample, was first thawed and then concentrated to a volume of 2 mL at 4000 rpm by using a Centriprep centrifugal concentrator with a molecular weight cutoff of 40 000. The 2 mL concentrates were then placed in Centricon concentrators with the same molecular weight cutoff. The sample volume was decreased to ~100 μL, resulting in a MMOH concentration of at least 1 mM. A small volume of mediator stock solution containing phenazine methosulfate, methylene blue, and potassium indigotetrasulfonate (10 mM in each, dissolved in H_2O) was added to achieve a 1 mM concentration of each mediator in the sample. The solution was placed in a vial, sealed with a septum, and then made anaerobic by repeatedly evacuating and back-filling with dioxygen-free argon. To reduce each batch, a small volume of a 0.1 M solution of sodium dithionite was added to achieve a final concentration of ~1 mM. The solutions were allowed to equilibrate for 30 min while being brought into an anaerobic chamber (Vacuum Atmospheres). Samples were then loaded into quartz tubes, capped with a septum, brought out of the box, and immediately frozen in liquid N_2. All tubes were stored in a liquid N_2 refrigerator before being shipped on dry ice from MIT to Northwestern University for ENDOR spectral studies.

In studies with dimethyl sulfoxide (DMSO), this reagent was added before the sample solution was made anaerobic. A concentration range of 50 mM to 0.2 M of DMSO was studied to monitor ENDOR spectral changes for native $MMOH_{mv}$ to fully bound $MMOH_{mv}$ + DMSO. Treatment of the protein with isotopically enriched DMSO (DMSO-d_6, 98%, Cambridge isotope Labs; ^{13}C-DMSO, 98% enriched, Isotech) was carried out in an identical manner.

Electron Nuclear Double Resonance Spectroscopy. Continuous wave (CW) ENDOR spectroscopy at 2 K was performed at a 35-GHz microwave frequency ("Q-band") on a locally constructed instrument described in more detail elsewhere[28] by using a TE_{011} cylindrical mode cavity equipped with mutually perpendicular field modulation and radio-frequency wires. In this study ENDOR signals are detected as radio-frequency-induced changes in the rapid-passage dispersion mode EPR signal.[19] The EPR signal is detected by using 100 kHz magnetic field modulation; the radio frequency is not modulated, but for broad ($\gtrsim$100 kHz) lines we have found an increase in signal by frequency-broadening the RF output.[29] The ENDOR transitions observed in this manner approximate the absorptive line shapes. For presentation, a baseline approximated by a slowly-varying polynomial function was subtracted from the CW ENDOR data.

Exchangeable ^{1}H resonances are characterized by comparison of CW signals from protein in H_2O and D_2O buffer and are facilitated by digital subtraction of the two signals. In our experience, this procedure is reliable for protons with resolved hyperfine couplings with $A(^{1}H) \gtrsim 2$ MHz. Subtracted CW spectra can show an artifactual amplitude near the center of the pattern, however, in which it appears that the intensity of proton ENDOR due to very weakly coupled protons ($A \leq 0.5$ MHz) is enhanced in the deuterated sample. This artifact in the difference spectrum is evidently due to a relaxation effect from the exchanged deuterons which enhances the amplitude of the "distant" proton ENDOR and makes it difficult to scale data for reliable subtractions. In this case, direct observation of the exchanged deuterons is important for analyzing the data. Resolved deuterium ENDOR is best obtained by pulsed ENDOR techniques.[30,31] Pulsed ENDOR at 35 GHz was performed on a locally constructed instrument to be described elsewhere.[32] We find that pulsed operation at the higher microwave frequency gives a dramatic increase in signal-to-noise ratio; this increase is especially advantageous for detection of weakly coupled nuclei. X-band ESEEM spectroscopy was performed on a locally constructed pulsed EPR spectrometer[33] operating at ~9.5 GHz, using a loop-gap

(24) Fox, B. G.; Hendrich, M. P.; Surerus, K. K.; Andersson, K. K.; Froland, W. A.; Lipscomb, J. D.; Münck, E. *J. Am. Chem. Soc.* **1993**, *115*, 3688−3701.

(25) Pilkington, S. J.; Dalton, H. In *Methods in Enzymology*; Academic Press: New York, 1990; Vol. 188, pp 181−190.

(26) Liu, K. E.; Johnson, C. C.; Newcomb, M.; Lippard, S. J. *J. Am. Chem. Soc.* **1993**, *115*, 939−947.

(27) Liu, K. E. Ph.D. Dissertation, Massachusetts Institute of Technology; Cambridge, MA, 1995.

(28) Werst, M. M.; Davoust, C. E.; Hoffman, B. M. *J. Am. Chem. Soc.* **1991**, *113*, 1533−1538.

(29) Hoffman, B. M.; DeRose, V. J.; Ong, Jui-L.; Davoust, C. E. *J. Magn. Reson., Ser. A* **1994**, *110*, 52−57.

(30) Fan, C.; Kennedy, M. C.; Beinert, H.; Hoffman, B. M. *J. Am. Chem. Soc.* **1992**, *114*, 374−375.

(31) Doan, P. E.; Fan, C.; Hoffman, B. M. *J. Am. Chem. Soc.* **1994**, *116*, 1033−1041.

(32) Davoust, C. E.; Doan, P. E.; Hoffman, B. M. *J. Magn. Reson.* In press.

(33) Fan, C.; Doan, P. E.; Davoust, C. E.; Hoffman, B. M. *J. Magn. Reson.* **1992**, *98*, 62−72.

resonator constructed for the same small (2 mm i.d.) samples used in Q-band spectroscopy.

Spectral Simulations. EPR spectra were simulated by using the program QPOW.[34] Orientation-selected, powder-pattern ENDOR spectra were simulated by using the program GENDOR.[19] Simulations of 3-pulse deuterium ESEEM were performed using a program described previously,[35] kindly provided by Prof. John McCracken (MSU), that incorporates the assumptions of an isotropic **g**-tensor and a spherical model for the contribution of multiple nuclei to the modulation pattern.

ENDOR Interpretation. A frozen-solution ENDOR spectrum obtained at magnetic field strength B_0 (for a single nucleus (N) of $I = {}^1/_2$) exhibits one or more doublets at frequencies $\nu_\pm$. The paired frequencies are given to first order by eq 2, where g_N and β_n are the

$$h\nu = |g_N\beta_n B_0 \pm A/2| = \nu_n \pm A/2| \quad (2)$$

nuclear g-value and nuclear magneton, respectively, and A is an electron−nuclear hyperfine coupling. The first term in (2), ν_N, is the Larmor frequency due to the nuclear Zeeman interaction at field strength B_0. Depending on the relative magnitudes of A and ν_N, the absolute value in eq 2 results in the two ENDOR transitions being either "Larmor-centered," i.e., centered at ν_N and separated by A, or "hyperfine centered", meaning centered at $A/2$ and separated by $2\nu_N$. Nuclei with $I > {}^1/_2$ are influenced by the nuclear electric quadrupole interaction, which further splits the two ENDOR transitions of eq 2, as described in eq 3, where the observed quadrupole splitting, $3P$, has a maximum of $3P_{max} = (3/2)e^2qQ$.[36]

$$\nu_\pm(m_I) = |g_N\beta_n B_0 \pm A/2 \pm (3P/2)(2m_I - 1)| \quad (3)$$

The powder-pattern EPR spectrum obtained from a frozen solution sample has contributions from all orientations of the paramagnetic center with respect to the external magnetic field. For a center having a **g**-tensor with rhombic symmetry ($g_1 > g_2 > g_3$), ENDOR spectra taken at the low-field (g_1) and high-field edges of the EPR envelope are "single-crystal-like", with each spectrum arising from only a single orientation of the molecules with respect to the magnetic field.[37] To determine fully a hyperfine tensor, including both the principal values and the orientation in the **g**-tensor axis frame, ENDOR data are collected and simulated at numerous points (g-values) across the EPR spectrum.[19]

Results

EPR Spectrum. A 35 GHz (Q-band) EPR spectrum of $MMOH_{mv}$ (*Mc*), obtained as the dispersion-detected rapid-passage signal, is shown in Figure 2a. The major component of the spectrum is simulated (dotted lines) with (g_1, g_2, g_3)=(1.94, 1.86, 1.74)[38] and line width parameters given in the figure legend.[34,39] The signal shows a slight heterogeneity near g_2 which is not due to contaminating amounts of protein B^{14} and is not associated with the component with (g_1, g_2, g_3) = (1.98, 1.87, 1.70) that has previously been reported as comprising ∼20% of the signal in $MMOH_{mv}$ from *M. trichosporium*.[15,24]

The X-band EPR signal of $MMOH_{mv}$ (*Mt*) in the presence of DMSO has been reported to be sharpened and less heterogeneous, with g-values of 1.95, 1.86, 1.77−1.79.[15,24] The Q-band EPR signal of $MMOH_{mv}$ (*Mc*) does appear sharpened in 200 mM DMSO (Figure 2b), but increased resolution at the higher microwave frequency discloses contributions from two components, neither being the native form. The simulation of the EPR signal in Figure 2b employed the following parameters: 70% of species 1 [(g_1, g_2, g_3) = 1.95, 1.87, 1.82)] and 30% of species 2 [(g_1, g_2, g_3) = (1.95, 1.85, 1.79)].

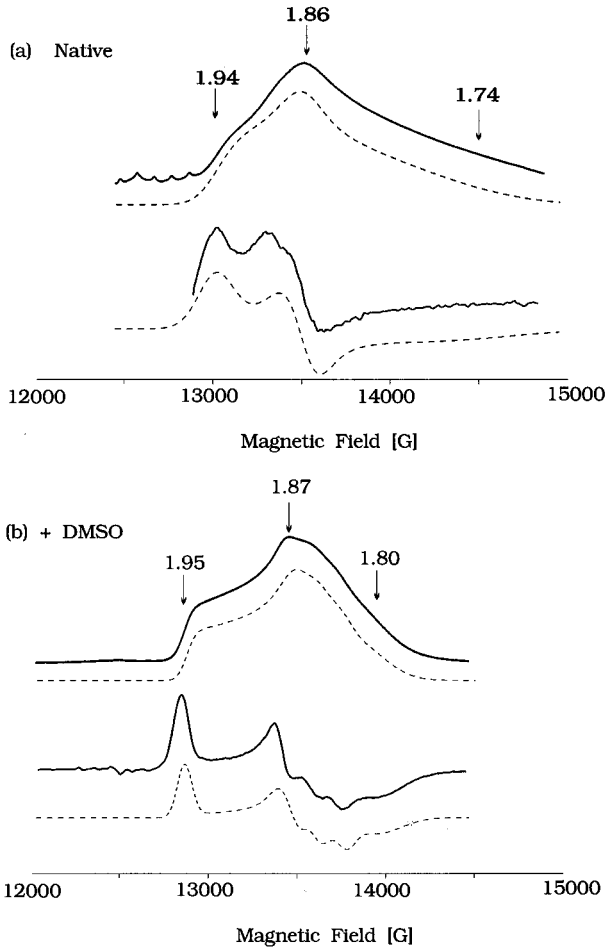

Figure 2. 35 GHz EPR spectra of $MMOH_{mv}$. Spectra are shown for (a) native $MMOH_{mv}$ and (b) $MMOH_{mv}$ treated with DMSO. In each case the rapid-passage dispersion-detected spectrum is shown (upper trace) along with the calculated derivative (lower trace). The spectrum of (a) native $MMOH_{mv}$ (*Mc*) is simulated (dotted line) using the following parameters: (g_1, g_2, g_3) = (1.940, 1.865, 1.740) and line width constants (see *Methods*)) = [300, 250, 450] MHz. The spectrum of $MMOH_{mv}$ + DMSO in (part b) was simulated (dotted line) by the addition of 70% species 1 [(g_1, g_2, g_3) = (1.948, 1.866, 1.816), line width (100, 140, 200) MHz] and 30% species 2 [(g_1, g_2, g_3) = (1.948, 1.845, 1.791), line width (180, 180, 250) MHz]. Spectrometer conditions: 2 K, 1.3 G (100 kHz) magnetic field MA, 3.2 mW microwave power, 64 ms time constant. Microwave frequency: (a) 35.295 GHz; (b) 35.175 GHz.

Proton ENDOR and the Effect of DMSO on Bound H_2O. Proton ENDOR patterns taken at g_1 (=1.94) for native $MMOH_{mv}$ (Figure 3) exhibit numerous ^1H doublets with $A(^1H) \leq 10$ MHz, at least two of which are exchangeable.[15,21] Table 1 lists all coupling constants. The non-exchangeable resonances are most likely due to the ring protons of the histidine ligands and possibly methylene protons of Glu. Comparison of the CW proton ENDOR spectra for native $MMOH_{mv}$ in H_2O and D_2O buffers (Figure 3a) shows an exchangeable ^1H doublet with A_{obs} = 7.8 MHz that has been assigned as a terminal H_2O (or hydroxide) ligand to the Fe^{2+} ion of the cluster, based on its hyperfine coupling;[21] this proton is more clearly seen in the digital subtractions (3b), which display features solely from

(34) Nilges, M. J. Ph.D. Dissertation, University of Illinois, Urbana, IL, 1979; EPR simulation program QPOW is available on request from R. L. Belford at the Illinois EPR Research Center.

(35) Magliozzo, R. S.; McCracken, J.; Peisach, J. *Biochem.* **1987**, *26*, 7923−7931.

(36) Wertz, J. E.; Bolton, J. R. *Electron spin resonance: elementary theory and practical applications*, 2nd ed.; Chapman and Hall: New York, 1986.

(37) Rist, G. H.; Hyde, J. S. *J. Chem. Phys.* **1970**, *52*, 4633−4643.

(38) These g-values differ slightly from the values of g = 1.92, 1.86, 1.71 reported previously for untreated $MMOH_{mv}$ (*Mc*) (ref 14).

(39) Bertrand, P.; More, C.; Guigliarelli, B.; Fournel, A.; Bennett, B.; Howes, B. *J. Am. Chem. Soc.* **1994**, *116*, 3078−3086.

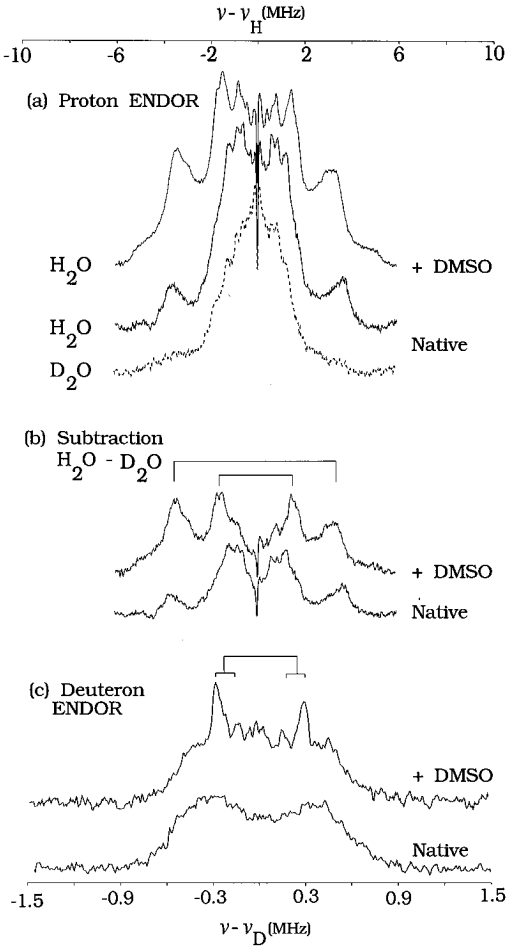

Figure 3. Proton and deuteron ENDOR at $g_1 = 1.94$ of native and DMSO-treated $MMOH_{mv}$. (a) CW proton ENDOR for DMSO-treated (a, top trace) and native (a, middle trace) $MMOH_{mv}$ in H_2O, and native protein in D_2O (a, lower trace; the DMSO-treated protein in D_2O has a similar proton ENDOR spectrum). (b) The [H_2O - D_2O] difference spectra are displayed for DMSO-treated (b, top trace) and native (b, lower trace) $MMOH_{mv}$. (c) Mims pulsed ENDOR spectra of the deuterated samples. The solid dashed lines in (b) and (c) indicate proton resonances from the aqua ligand; the dotted line corresponds to a second exchangeable proton. Spectra in (a) and (b) are centered at the proton Larmor frequency (upper axis) and spectra in (c) are centered at the deuterium Larmor frequency (lower axis). To compare the proton and deuteron spectra, the width of the lower axis for the deuteron spectra is scaled to that of the proton spectra by the ratio of the proton-deuteron Larmor frequencies, ~1/6.5. *Conditions:* (a) 35.1 GHz microwave frequency, $g = 1.94$, 0.17 G modulation amplitude, 3.2 mW microwave power, 25 W rf power, 0.5 MHz rf scan rate (negative sweep direction), average of 470 (native, H_2O), 60 (DMSO-treated, H_2O), and 175 (native, D_2O) scans. (c) Mims pulsed ENDOR sequence with $\tau = 500$ ns, $\pi/2$ $t_p = 32$ ns, rf $t_p = 60$ μs, 30 ms repetition rate, 2 K, 512 points/scan. (DMSO-treated) 34.643 GHz, 12690 G, average of 1440 transients; (native) 34.695 GHz, 12776 G, average of 990 transients.

exchangeable protons. As confirmation, the deuteron Mims Q-band pulsed ENDOR of $MMOH_{mv}$ in D_2O (3c) shows a pattern of resonances the width of which matches that expected for the exchangeable H_2O signal observed in the subtracted CW proton ENDOR spectrum.

As seen in Figure 3, the $^{1,2}H$ ENDOR spectra for DMSO-treated $MMOH_{mv}$ in H_2O and D_2O buffer are quite similar to those for native $MMOH_{mv}$, although the resonances appear sharper and the couplings have slightly different values (listed in Table 1). Again, there is the clear presence of an exchangeable ^1H signal from bound H_2O, with Mims pulsed deuteron ENDOR (Figure 3c) confirming the CW $H_2O - D_2O$ difference spectrum. The deuteron ENDOR spectra for DMSO-treated $MMOH_{mv}$ show sharper features; for example, quadrupole splitting of a second deuteron corresponding to $A(^1H) \sim 3$ MHz is now resolved in the doublet of doublets that can be assigned to $A(^2H) = 0.42$ MHz with $3P \sim 0.14$ MHz.

Table 1. Observed Proton Hyperfine Coupling Constants for $MMOH_{mv}$[a]

$A < 5$ MHz	A_{obs} at g_1 (MHz)
native	0.2, 0.4, 0.9, 1.2, 1.8, 2.3*, 2.5*, 3.4
+ DMSO	0.2, 0.8, 1.4, 1.6, 3.0*, 3.4
$A < 10$ MHz	A_{obs} at (g_1, g_2, g_3)[b] (MHz)
native	7.4*
+ DMSO	6.0*, 7.0*
$A > 10$ MHz	A_{obs} at (g_1, g_2, g_3)[b] (MHz)
native	(14*, 30*, 24*)
+ DMSO	(14*, 30*, 24*)

[a] An asterisk indicates protons that exchange in D_2O. [b] Values given are for maximum observed hyperfine couplings at a given g value.

These spectra thus show that DMSO does not bind at Fe^{2+} by replacement of H_2O.

^{1}H ENDOR of the OH^- Bridge. We previously reported that the $MMOH_{mv}$ proton ENDOR spectra obtained with protein isolated from both *M. trichosporium* OB3b and *M. capsulatus* (Bath) contain a set of very unusual, strongly coupled, exchangeable proton resonances that could be assigned as the signals of a bridging hydroxide ligand.[21] The ENDOR spectra in Figure 4 show the signals from this bridge proton for $MMOH_{mv}$(*Mc*) taken at the three canonical g values. These spectra were collected under conditions that accentuate broad hyperfine resonances with large couplings at the cost of resolution in the weak and intermediate coupling regions. Characteristics of these hydroxo-bridge resonances are without precedence: they are highly anisotropic, with a hyperfine coupling of $A \sim 14$ MHz at g_1 and intensity extending to $A \sim 30$ MHz at g_2 and $A \sim 24$ MHz at g_3.[40,41] The DMSO-treated sample also exhibits bridge resonances with essentially the same characteristics (Figure 4); the signals appear sharper near g_2 and g_3 in the DMSO-treated sample because of the sharper and more axial line shape of the EPR signal. Thus, treatment with DMSO does not strongly perturb the hydroxo bridge of the mixed-valence center.[42,43]

Nitrogen ENDOR of $MMOH_{mv}$ and DMSO-Treated $MMOH_{mv}$ at g_1. The properties of the two histidyl ligands bound to the diiron center have been examined through CW Q-band nitrogen ENDOR spectra for the ^{14}N (natural abundance)

(40) The extreme hyperfine anisotropy contributes to the low relative amplitude of the hydroxide-bridge proton ENDOR signals. Such signals were not detected in previous CW ENDOR studies of either $MMOH_{mv}$(*Mt*) (ref 15) or the dinuclear center of uteroferrin (ref 41). In the case of uteroferrin, however, an ESEEM study of deuterium-exchanged samples reported deuteron frequencies corresponding to very strongly coupled protons. It was speculated that such strongly coupled protons, predicted from the ESEEM data to have $A(^1H,g_2) \sim 14$ MHz and $A(^1H,g_3) > 20$ MHz, might be due to a hydroxide bridge in reduced uteroferrin (ref 41).

(41) Doi, K.; McCracken, J.; Peisach, J.; Aisen, P. *J. Biol. Chem.* **1988**, *263*, 5757−5763.

(42) There has also appeared a pulsed ENDOR and ESEEM study on DMSO-treated $MMOH_{mv}$(*Mt*) (ref 43) that supports our conclusions concerning the MMOH hydroxide bridge, but in which the stated hyperfine couplings conflict with the data shown in Figure 4. In that study, the hyperfine coupling predicted for g_1 was 23 MHz and that for g_2 was 14 MHz; these values clearly fail to match the values directly observed in this study and shown in Figure 4, which are 14 MHz at g_1 and ~30 MHz at g_2. See ref 22 for an additional discussion of $MMOH_{mv}$ ESEEM results.

(43) Thomann, H.; Bernardo, M.; McCormick, J. M.; Pulver, S.; Andersson, K. K.; Lipscomb, J. D.; Solomon, E. I. *J. Am. Chem. Soc.* **1993**, *115*, 8881−8882.

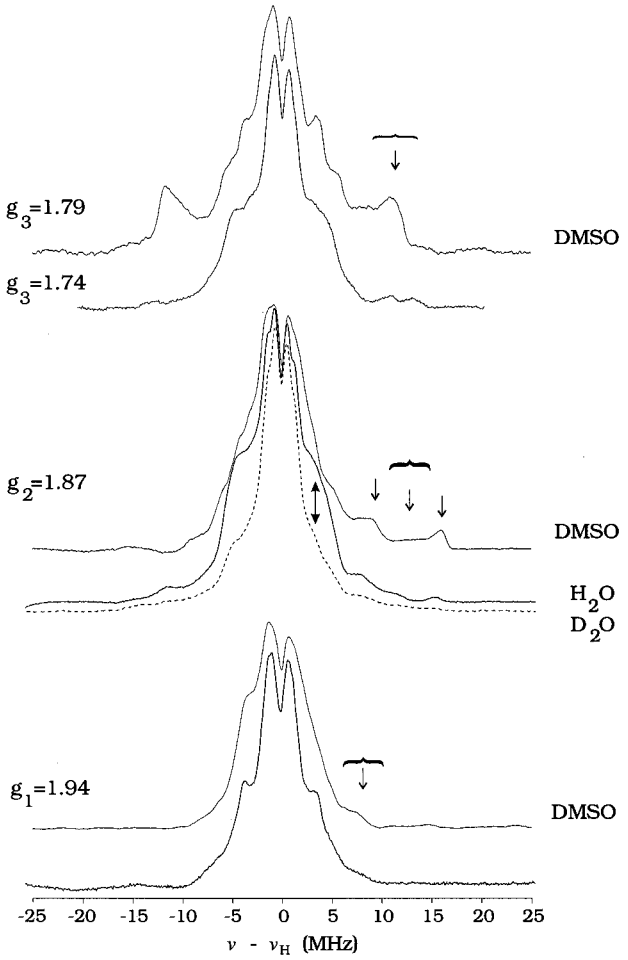

Figure 4. Field dependence of ^{1}H ENDOR due to the strongly-coupled bridge proton in $MMOH_{mv}$. Resonances assigned as the hydroxide bridge in native and DMSO-treated $MMOH_{mv}$ are shown (arrows and brackets) for field positions corresponding to g_1 (bottom), g_2 (middle), and g_3 (top). In each case the top trace is +DMSO; at g_2 both native in H_2O and D_2O (dotted line) are shown. Data are shown centered at the proton Larmor frequency for each scan. *Spectrometer conditions:* 35.02 GHz, *g*-values as shown, 3.2 mW microwave power, 1.3 G modulation amplitude, 1 MHz/s rf scan rate (negative sweep), 200 kHz rf bandwidth.

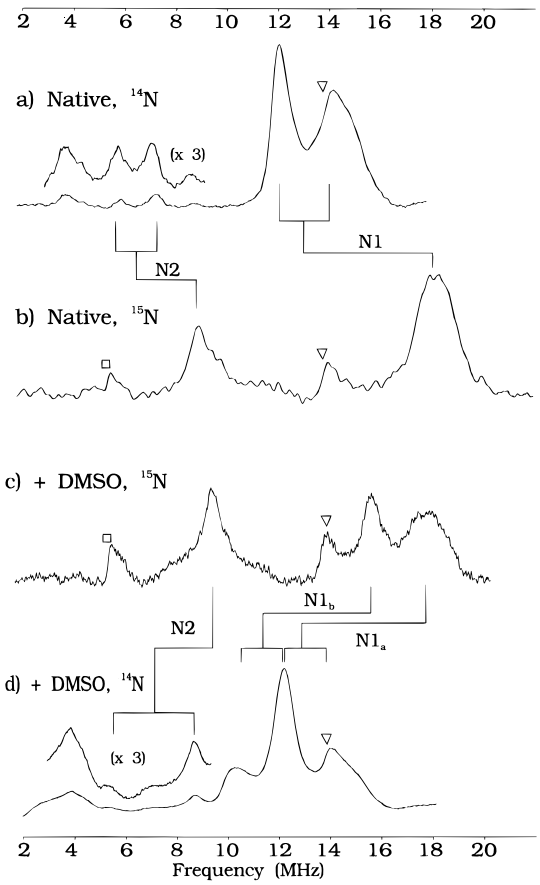

Figure 5. Nitrogen ENDOR at g_1 of $MMOH_{mv}$. Data are shown for (a, d) natural-abundance ^{14}N and for (b,c) ^{15}N-labeled $MMOH_{mv}$. Traces a and b are of native $MMOH_{mv}$ whereas traces c and d are of $MMOH_{mv}$ in the presence of 0.2 M DMSO. ENDOR transitions assigned to N1 and N2 are marked by lines and vertical bars. The ν_+ transitions (see text) for ^{15}N are connected to respective quadrupole-split ^{14}N resonances. "Hyperfine-centered" doublets (N1) are centered at $A/2$ and separated by $2\nu_N$; "Larmor-centered" doublets (N2) are centered at ν_N and are separated by A. The symbols (▽ and □ respectively) indicate resonances at the Larmor frequency of ^{13}C (a−d) and ^{15}N (b, c), due to the "distant" ENDOR effect (see text). *Conditions:* 0.3 G modulation amplitude, 1 MHz/s rf scan, positive sweep, 32 ms time constant, 3.2 mW microwave power, 30 W rf power, 200 kHz rf bandwidth: (a) 35.02 GHz, 12920 G, average of 320 scans; (b) 35.09 GHz, 12950 G, average of 190 scans; (c) 34.90 GHz, 12800 G, average of 50 scans; (d) 35.10 GHz, 12870 G, average of 260 scans.

and ^{15}N-enriched protein, both in the native form and in the presence of DMSO. This experiment is of particular importance because it had been reported that addition of DMSO caused no change to the His bound to Fe^{3+}, but resulted in the loss of the ENDOR signal from the ^{14}N of His bound to the Fe^{2+} site.[15]

The ^{15}N ENDOR spectrum of native $MMOH_{mv}$ obtained at $g_1 = 1.94$, Figure 5b, is assigned as ν_+ transitions of the two histidyl nitrogen nuclei (N1 and N2) coupled to the electron spin. As described elsewhere,[19,28] in Q-band ENDOR it is not uncommon to observe only ν_+ for a given ENDOR doublet. Through the use of eq 2 and the appropriate value $\nu(^{15}N) = 5.6$ MHz, the hyperfine couplings are $A(^{15}N1) = 25.0$ MHz and $A(^{15}N2) = 6.8$ MHz (Table 2). These ^{15}N assignments at g_1 correlate with the positions of the corresponding quadrupole-split ^{14}N resonances for ^{14}N $MMOH_{mv}$, Figure 5a; the ^{15}N ($I = {}^1/_2$) and ^{14}N ($I = 1$) Larmor frequencies and hyperfine couplings are related by the ratios of the nuclear moments, with $\nu_n(^{15}N)/\nu_n(^{14}N) = A(^{15}N)/A(^{14}N) = 1.4$. The observed ^{14}N quadrupole splittings (eq 3) give $3P(N1) \cong 3P(N2) \cong 1.8$ MHz. The derived hyperfine couplings for ^{14}N1 and ^{14}N2 are in agreement with earlier X-band ^{14}N results obtained on $MMOH_{mv}$ (*Mt*).[15] As discussed below, the hyperfine tensor elements of a ligand atom to the ferric site in the spin-coupled, mixed-valence diiron center are expected to be substantially larger than those of a ligand to the ferrous site. As $A(N1) > A(N2)$, N1 and N2 can be assigned as the histidine ligands bonded to the ferric and ferrous site, respectively.

Table 2. ^{15}N Hyperfine Coupling Parameters for $MMOH_{mv}$

		A_{obs} [a] at g_1	A_1	A_2	A_3	a_{iso}	ϕ, θ [b]
$MMOH_{mv}$	N1	25	22	22	29.5	23	0, 35
	N2	6.8	6	7	9	8	0, 0
+ DMSO	$N1_a$	24					
	$N1_b$	20					
	N2	7.8	8	7	8	8	*c*

[a] Hyperfine couplings given in MHz. Errors due to sweep artifacts are ~±0.5 MHz. [b] Euler angle relating **A** tensor to ***g***. The third Euler angle, ψ, cannot be determined. [c] Treated as coaxial with **g**.

The nitrogen ENDOR spectra for DMSO-treated ^{14}N and ^{15}N-labeled $MMOH_{mv}$ are shown in Figure 5c,d. Comparison of the ^{15}N spectra without (Figure 5b) and with (5c) DMSO shows that this exogenous ligand perturbs both N2 bound to the ferrous ion, and N1 bound to the ferric ion. For the latter, DMSO

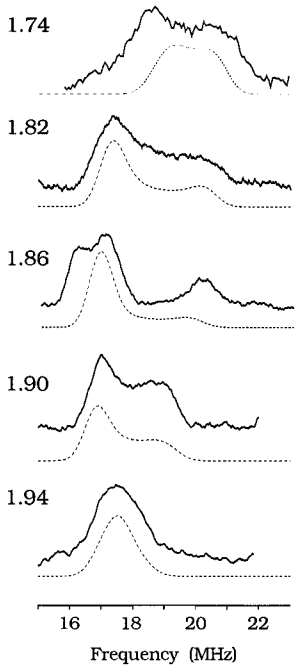

Figure 6. Orientation dependence of ν_+ (^{15}N1) resonances from native MMOH$_{mv}$. The ν_+ (^{15}N) resonance of N1 from native MMOH$_{mv}$ is shown at several *g*-values across the EPR envelope. The data are simulated (dotted lines) with parameters described in Table 1. *Conditions:* 35.1 GHz (*g*-values as shown), other conditions as in Figure 2 except that the scan rates were 0.5−1 MHz/s and in the *negative* sweep direction; averages of 200−300 scans each.

treatment clearly leads to two different N1 resonances, denoted N1$_a$ and N1$_b$; one has a larger and one has a smaller (Table 2) hyperfine coupling than N1 in the unperturbed protein. Because the **g**-tensor of EPR species 2 and the hyperfine value of N1$_b$ in DMSO-treated enzyme differ most from those of native MMOH$_{mv}$, we provisionally associate them with one another. Thus, in contrast to the earlier report,[15] the histidines bound to both iron ions are both perturbed by the interaction of DMSO with MMOH$_{mv}$(*Mc*), and the histidine bound to the ferrous ion clearly is not lost as a ligand.

This assignment of the ^{15}N spectra of DMSO-treated MMOH$_{mv}$ leads to a consistent interpretation of the corresponding ^{14}N spectra, and the ^{14}N data (Figure 5d) give quadrupole couplings of $3P(N1_a) \simeq 1.2$, $3P(N1_b) \approx 1.9$, and $3P(N2) \approx 3.6$ MHz. The value for 3P(N2) is the maximum expected for Fe-bound His ^{14}N,[44,45] and would require that g_1 lies roughly along the Fe−N2 bond in DMSO-treated MMOH$_{mv}$. Because the principal values of the quadrupole tensor of ^{14}N(His) bound to Fe are not highly sensitive to the nature of the active site, a significant change in the value of P(N2), observed at g_1, from 1.9 to 3.6 MHz, upon DMSO-treatment of MMOH$_{mv}$ would indicate a change in the relative orientations of the His imidazole and **g**-tensor frames upon treatment with the exogenous ligand.

Field-Dependent ^{15}N ENDOR Spectroscopy. To examine the metal−ligand bonding in greater detail, full ^{15}N hyperfine tensors were obtained for native and DMSO-treated MMOH$_{mv}$ by analysis of ENDOR spectra collected at numerous *g*-values across the EPR spectrum. As shown in Figure 6, the single, broad ν_+ peak at $g_1 = 1.94$ for ^{15}N1 of the native enzyme, corresponding to $A = 25$ MHz, smoothly resolves into multiple resonances as the field is increased (g decreased); these resonances reconverge at the lowest *g*-values, where $A \sim 28$ MHz. Simulation of the data for ^{15}N1 (as described under Methods) indicates an essentially axial hyperfine tensor with principal values of $A_{1,2,3} = (22.0, 22.0, 29.5)$ MHz. The direction of the largest tensor component, A_3, which corresponds to the Fe−N vector for histidine bound to high-spin Fe^{3+},[45] lies in the g_1-g_3 plane and is rotated away from g_3 by ∼30° (Table 2);[46] however, the extent to which A_3 is rotated out of the g_1-g_3 plane is not well-determined, and could be as much as 35°. The analogous field-dependence of the ^{15}N2 ENDOR pattern for native MMOH$_{mv}$ (data not shown) could roughly be simulated by collinear $\boldsymbol{g}-$ and **A**-tensors, with $A_{1,2,3} = (6.4, 7.3, 9.3)$ MHz. Because the ENDOR lines at fields away from g_1 are broad and poorly resolved, the tensor components are moderately reliable, but the orientation is not.

Field-dependent ^{15}N ENDOR spectra of DMSO-treated MMOH$_{mv}$ (supporting information, Figure S1) are distinctly different from those of the native sample at all fields. Simulations confirm that these differences are due to a change of both the N1 and N2 hyperfine tensor principal values,[47] and thus reflect changes in bonding at the iron sites.

These ^{14,15}N ENDOR data thus show that treatment of MMOH$_{mv}$ with DMSO causes small changes at the ferrous site, but a distinct alteration in the coordination environment about the ferric site as manifested by the occurrence of two forms of MMOH$_{mv}$ with distinguishable hyperfine couplings for His N1 bound to ferric ion.

^{57}Fe ENDOR of MMOH. ^{57}Fe ENDOR patterns collected for the dinuclear iron cluster of isotopically labeled native and DMSO-treated MMOH$_{mv}$ are presented in Figure 7. At g_1, each of the MMOH$_{mv}$ samples shows two strong sets of hyperfine-centered ^{57}Fe resonances (eq 2; $2\nu_N(^{57}Fe) \lesssim 4$ MHz), one corresponding to A(Fe1) ∼ 62 MHz and the other to A(Fe2) ∼ 36−38 MHz (Figure 7). The previous X-band ^{57}Fe ENDOR study of MMOH$_{mv}$(*Mt*)[24] reported ferric-site values at g_1 and g_2 that are in good agreement with those obtained here. As described in more detail below, Fe1 is assigned as the ferric site and Fe2 as the ferrous site.

^{57}Fe ENDOR data for both sites were collected at field values across the EPR envelope (supporting information, Figures S2 and S3). The **A** tensors derived from these data for enzyme with and without DMSO are coaxial with **g** and have principal values listed in Table 3. Mössbauer data for the ferrous ion of DMSO-treated MMOH$_{mv}$ (*Mt*) give tensor components similar to those reported here,[24] although without the orientational information. The hyperfine tensor for the ferric site has a large isotropic component, ∼69 MHz, and a small but readily measured anisotropy. The hyperfine tensor of the ferrous site, as expected,[24] is highly anisotropic.

Neither the spectra at g_1 nor the full hyperfine tensors change when MMOH$_{mv}$ is treated with DMSO (Figure 7b; Table 3). In particular, the tensor orientations do not change: in both cases the ferrous tensor is pseudoaxial with its unique (small) value along g_3.

ENDOR and ESEEM of ^{13}C and ^{2}H Labeled DMSO. As described in the previous sections, treatment with DMSO changes the EPR spectrum of MMOH$_{mv}$, but causes only minor

(44) Gurbiel, R. J.; Batie, C. J.; Sivaraja, M.; True, A. E.; Fee, J. A.; Hoffman, B. M.; Ballou, D. P. *Biochemistry* **1989**, *28*, 4861−4871.

(45) Scholes, C. P.; Lapidot, A.; Mascarenhas, R.; Inubushi, T.; Isaacson, R. A.; Feher, G. *J. Am. Chem. Soc.* **1982**, *104*, 2724−2735.

(46) As can be seen in Figure 4a, this simulation successfully reproduces the breadth and overall pattern of the ENDOR resonances. A small additional splitting of the lower-frequency components near g_2 is not reproduced, however. This splitting can be simulated by an additional rotation of the **A** tensor about **g**, but the additional spectral features could also be due to the EPR signal heterogeneity.

(47) However, the heterogeneity of the EPR spectra from DMSO-treated MMOH$_{mv}$ seen in Figure 2 precluded a fully satisfactory tensor determination.

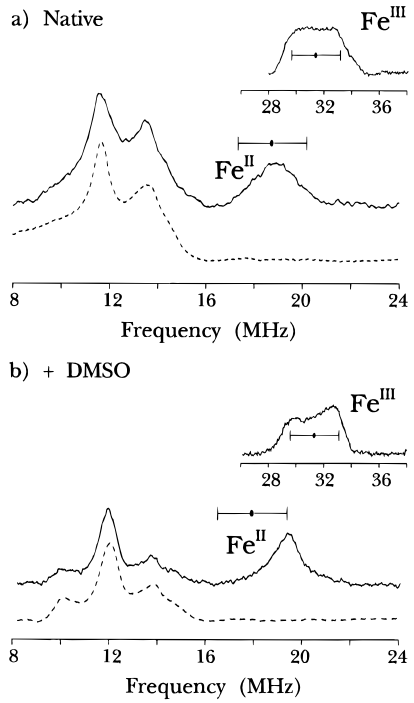

Figure 7. ^{57}Fe ENDOR of the iron sites in $MMOH_{mv}$. ^{57}Fe ENDOR spectra obtained at g_1 are shown for (a) $MMOH_{mv}$ and (b) $MMOH_{mv}$ treated with DMSO. Solid lines are of ^{57}Fe-labeled samples, and dotted lines show background in the absence of ^{57}Fe. ^{57}Fe transitions are centered at $A/2$ (solid circles) and split by $2\nu_n(^{57}Fe)$ (horizontal bars). The insets show ^{57}Fe ENDOR for the Fe^{+3} site, at higher frequency. *Conditions:* 35.2 GHz, 0.3 G MA, 1 MHz rf scan rate (negative sweep), 200 kHz rf bandwidth, averages of 50−200 sweeps.

perturbations of the constitutive nuclei of $MMOH_{mv}$, thereby leaving its mode of interaction unclear. We therefore investigated $MMOH_{mv}$ treated with DMSO labeled with ^{2}H (DMSO-d_6) or ^{13}C at the methyl groups. The couplings from nuclei of the DMSO methyl groups are expected to be small whether or not the molecule is a metal ligand, and not surprisingly the ^{13}C and ^{2}H CW ENDOR signals are unresolved (data not shown) and give no detailed information. Fortunately, the Mims pulsed ENDOR technique is highly effective in resolving transitions from weakly coupled nuclei,[31] and the enhanced sensitivity of the Q-band spectrometer relative to those operating at X band[32] permits this technique to be applied to $MMOH_{mv}$.

Figure 8 shows Q-band Mims pulsed ENDOR from ^{2}H and ^{13}C in samples prepared with labeled DMSO. These spectra, shown centered at the respective Larmor frequencies, have their maximum breadths at $\sim g_2$, with maximum hyperfine couplings of ∼1.3 MHz for the ^{13}C nuclei and ∼1.0 MHz for the ^{2}H samples. At g_1 the deuteron spectra show two resolved doublets, separated by ∼0.2 MHz. This splitting is within the maximum expected for quadrupole splittings ($3P_{max}$ ∼0.3 MHz),[48] but could also arise from orientation selection and/or two different populations of deuterons. The mere existence of such well-defined structure in the ^{2}H ENDOR pattern requires that the deuterated methyl groups of DMSO have defined orientations with respect to the dinuclear Fe center, suggesting an ordered binding site. The fact that the ^{13}C and ^{2}H spectra show the same field dependence, with maximum couplings near g_2 that are roughly in the ratio of A_C/A_D $\sim g_C/g_D$ ∼1.6, confirms the expectation that these couplings arise from the through-space electron−nuclear dipolar interaction. Since this interaction has a well-defined dependence on metrical parameters, this interpretation permits the use of these hyperfine couplings to investigate the geometry of DMSO binding (*vide infra*).

The frequencies of the well-resolved ^{2}H ENDOR spectra give the hyperfine couplings, but the spectra do not indicate whether the resonances arise from one or both CD_3 groups of a DMSO molecule. Electron spin−echo envelope modulation (ESEEM) spectra can in principle be used to quantitate deuterons[49] and so such data were collected. The X-band 3-pulse ESEEM of the DMSO-d_6 $MMOH_{mv}$ sample shows deep modulation due to nearby deuterons (Figure 9). These data were well simulated[35,49] in both frequency and depth by using the approximations described under Methods, and by assuming a point dipole approximation for the hyperfine coupling (Figure 9b). The hyperfine parameters used in Figure 9b,c were chosen to be consistent with the maximum breadth of ∼1.0 MHz for the Mims deuteron ENDOR pattern shown in Figure 8a. The ESEEM spectral simulations are indeed very sensitive to the number of contributing deuterons. The simulation for three deuterons more closely resembles the experimental data both in the time domain pattern and, perhaps more easily observed, the Fourier transforms shown in Figures 9e and 9f, where an increase in the amplitudes of the first and second harmonics of the deuteron frequency is seen in the simulation with six deuterium nuclei. The fact that the ESEEM modulation of DMSO-d_6 treated $MMOH_{mv}$ is better simulated by a contribution of only three deuterium nuclei suggests that the DMSO is arranged asymmetrically with respect to the dinuclear Fe center, such that the closer methyl group dominates the ESEEM spectrum.

Analysis

Cluster Spin Coupling. The mixed-valence, $Fe^{2+}(S = 2)$−$Fe^{3+}(S = {}^5/_2)$ carboxylate-bridged center of $MMOH_{mv}$ displays antiferromagnetic coupling and an $S = {}^1/_2$ ground state. To relate the hyperfine parameters derived in this study to structural parameters, the cluster spin coupling must be taken into account. For strong antiferromagnetic coupling, the interaction of the cluster $S = {}^1/_2$ electron spin with the external field can be described with a cluster **g** tensor that in turn can be written in terms of the $\mathbf{g}^i$ tensors of the individual iron ions,[50] where the

$$\mathbf{g} = {}^7/_3\mathbf{g}^a - {}^4/_3\mathbf{g}^b \tag{4a}$$

a and b superscripts correspond to ferric and ferrous sites, respectively. For the approximately isotropic d^5 ferric site, the $\mathbf{g}^a$ tensor parameters show little change with coordination environment and can generally be approximated by an isotropic value of $\mathbf{g} = 2$.[24,51] The spin parameters for the ferrous site, however, can be greatly affected by the ligand environment, giving rise to relatively anisotropic local **g**-tensors. Given this variability, it is generally considered that differences in the cluster g values among members of this class of coupled dinuclear center are related to differences in the environment of the ferrous site.[52,53]

A nucleus, α, that has hyperfine couplings to the individual iron ions of $\mathbf{a}^i(\alpha)$ has a hyperfine coupling of $\mathbf{A}(\alpha)$ to the cluster spin (eq 4b). When a nucleus couples only to the spin of one

(48) Ragle, J. L.; Mokarram, M.; Presz, D.; Minott, G. *J. Magn. Reson.* 1975, *20*, 195−213.

(49) Mims, W. B.; Peisach, J. In *Advanced EPR. Applications in Biology and Biochemistry*; Hoff, A. J., Ed.; Elsevier: Amsterdam, 1989; pp 1−57.

(50) Hagen, W. R. *Adv. Inorg. Chem.* **1992**, *38*, 165−222.

(51) Sage, J. T.; Xia, Y.-M.; Debrunner, P. G.; Keough, D. T.; de Jersey, J.; Zerner, B. *J. Am. Chem. Soc.* **1989**, *111*, 7239−7247.

(52) Bertrand, P.; Guigliarelli, B.; More, C. *New J. Chem.* **1991**, *15*, 445−454.

(53) More, C.; Bertrand, P.; Gayda, J. P. *J. Magn. Reson.* **1987**, *73*, 13−22.

Table 3. ^{57}Fe Hyperfine Constants

		A_1	A_2	A_3	a_{iso}	(g_1, g_2, g_3)	ref
$MMOH_{mv}$[a]							
M. capsulatus	Fe^{2+}	38	38	n.d.	n.d.	(1.94, 1.86, 1.74)	this work
	Fe^{3+}	62	68	76	69		
+ DMSO[a]	Fe^{2+}	36	38	<20	<31	(1.95, 1.87, 1.82)	this work
	Fe^{3+}	62	68	76	69		
M. trichosporium	Fe^{2+}	34.3	36.5	17.9	29.5	(1.95, 1.86, 1.79)	24
+ DMSO[b]	Fe^{3+}	63	69	74	69		

[a] **A** and **g** are coaxial. Correspondence between components is determined from ENDOR measurements. [b] Magnitudes determined from Mössbauer measurements; tensor directions are arranged to match ENDOR measurements in this work.

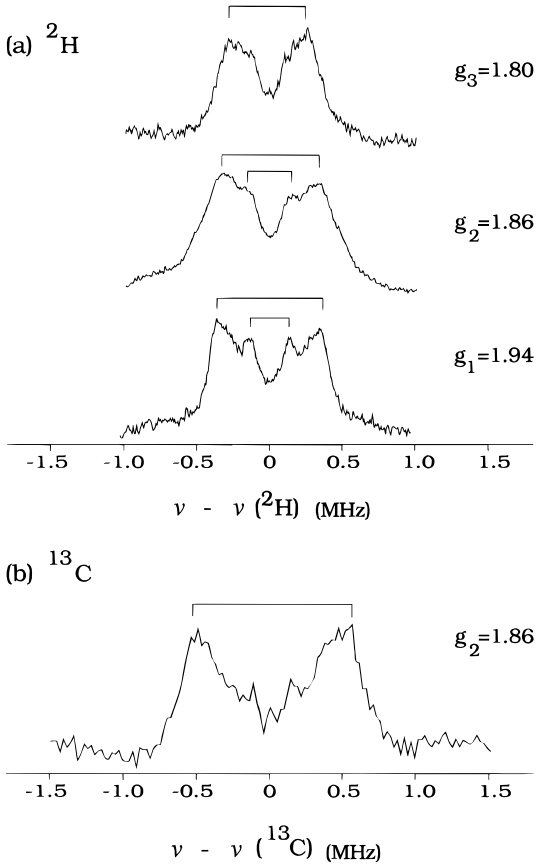

Figure 8. Q-band Mims pulsed ^{2}H, ^{13}C ENDOR of $MMOH_{mv}$ plus isotopically labeled DMSO. (a) ^{2}H ENDOR from $MMOH_{mv}$ treated with deuterated DMSO are displayed for three *g*-values. (b) ^{13}C Mims ENDOR from $MMOH_{mv}$ + ^{13}C-DMSO collected at $g_2 = 1.86$. In all spectra, the horizontal bars indicate hyperfine splittings (see text) and spectra are centered at the ^{2}H, ^{13}C Larmor frequencies. *Conditions:* $\pi/2$ $t_p = 24$ ns, rf $t_p = 60$ μs, 512 points/scan, 30 ms repetition rate, ~480 transients for each scan. (a) 34.586 GHz, $\tau = 468$ ns; (b) 34.738 GHz, $\tau = 444$ ns.

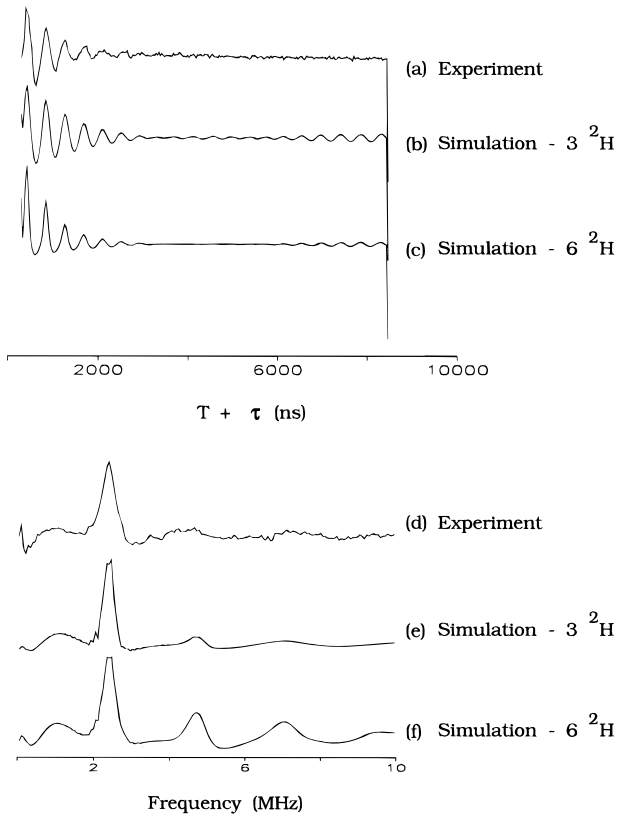

Figure 9. ^{2}H ESEEM of $MMOH_{mv}$ plus deuterated DMSO. X-band ESEEM data were obtained at $g = 1.85$. The time-domain (a−c) and Fourier transformed frequency-domain (d−f) data are shown. The data are compared with simulations (see text) including either three (b, e) or six (c, f) deuterons. *Conditions:* 9.434 GHz, 3635 G, 3-pulse ESEEM sequence with $\tau = 192$ ns, $\pi/2$ $t_p = 16$ ns, time *T* between first and second pulses stepped in 32 ns increments for 256 points, 50 ms sequence repetition rate, average of 140 transients. Simulations were performed as described under *Methods*, with $a_{aniso} = 0.5$ MHz.

$$\mathbf{A}(\alpha) = {}^{7}/_{3}\mathbf{a}^{a}(\alpha) - {}^{4}/_{3}\mathbf{a}^{b}(\alpha) \qquad (4b)$$

Fe ion, only one term contributes to eq 4b. For example, the observed ^{57}Fe hyperfine coupling of the ferric site would be related to the hyperfine coupling in a mononuclear center by $\mathbf{A}^a = {}^{7}/_{3}\mathbf{a}^a$. A nucleus that has appreciable interaction with the electronic spin from both ferric and ferrous sites, such as the hydroxo bridge proton, would have non-zero $\mathbf{a}^a$ *and* $\mathbf{a}^b$ in eq 4 (*vide infra).*

When the strong-coupling limit is not attained, then corrections to eqs 4 must be included due to mixing of low-lying excited states. Such corrections were found to be necessary in analyzing ^{57}Fe Mössbauer data for the carboxylate-bridged dinuclear Fe center of purple acid phosphatase ($J \sim 20$ cm^{-1})[51] and are employed for the $MMOH_{mv}$ ($J \sim 60$ cm^{-1}) ^{57}Fe ENDOR data in Appendix II. The strong-coupling approximations of eq 4 are sufficient, however, in the analysis of $MMOH_{mv}$ ligand hyperfine interactions.

Analysis of Hydroxide-Bridge ENDOR. The initial assignment of the unusual exchangeable ^{1}H proton resonances of Figure 4 to an OH^- bridge was based on comparisons between $MMOH_{mv}$ and N_3Hr_{mv}.[21] In this section we show that these ^{1}H ENDOR patterns can be understood in terms of a cluster hyperfine tensor, **A**, that is the weighted sum of point-dipole interactions between a bridge proton and the localized spins on the two iron ions. We begin by considering an idealized but realistic geometry for the Fe(OH)Fe moiety, as depicted in Figure 10. The unit is taken as symmetrical, with all four atoms

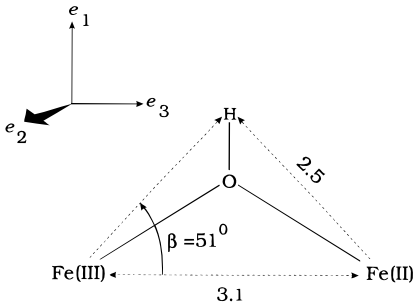

Figure 10. Geometry used in simulating proton ENDOR from the hydroxide bridge of $MMOH_{mv}$. Distances (in Å) as shown.[54] A molecular axis system, having principal directions (e_1, e_2, e_3) and oriented such that e_3 is parallel to the Fe−Fe vector and e_2 is perpendicular to the Fe−OH−Fe plane, is shown in the upper left hand corner.

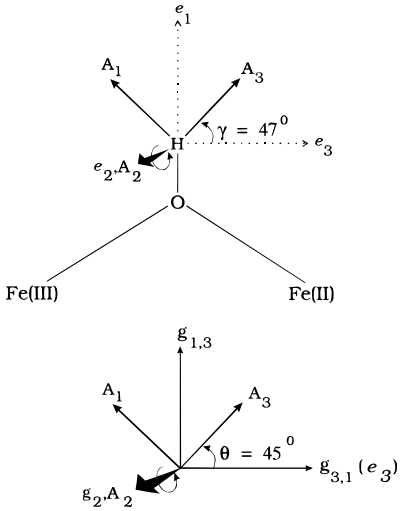

Figure 11. Orientation of the proton **A** tensor from the hydroxide bridge of $MMOH_{mv}$. Upper: The principal axis system of the calculated dipolar **A** tensor of the hydroxide bridge proton (see Appendix I) is shown in relation to the molecular *e*-tensor as defined in Figure 10. Lower: The orientation of this **A** tensor with respect to the *molecular g*-tensor, as determined by simulations of the proton ENDOR spectrum (Figure 12), is shown. Comparison shows that the axes are parallel, with e_2 and g_2 axes collinear. As depicted in the figure, the data can not distinguish between g_1 being collinear with e_1 or e_3; however, in the text a preference for g_1 collinear with e_3 is discussed.

lying in a plane and with the metrical parameters as indicated.[54] It is convenient to define a right-handed coordinate frame (**e**), the unit vectors of which are the following: e_3, lying along Fe−Fe; e_1, lying in the plane perpendicular to e_3; and e_2, normal to the plane.

One can use the classical form of the point-dipole interaction in conjunction with the spin coupling relationship of eq 4b to calculate the hydroxo bridge proton ENDOR frequencies for a particular molecular orientation of the molecular geometry of Figure 10 in an external magnetic field. Such calculations, described in Appendix I, predict a dipolar hyperfine tensor with principal components $A = [-25, -5, +30]$ MHz and an orientation as shown in Figure 11. The predicted principal values were used without adjustment to simulate (see Methods) the field-dependent experimental proton ENDOR data of Figure 4. As illustrated for native $MMOH_{mv}$ in Figure 12, in both enzyme forms the simulations reproduce the experimental data extremely well when this hyperfine tensor is related to the **g**

(54) These metrical parameters are arrived at by adopting the structure displayed in Figure 1B.

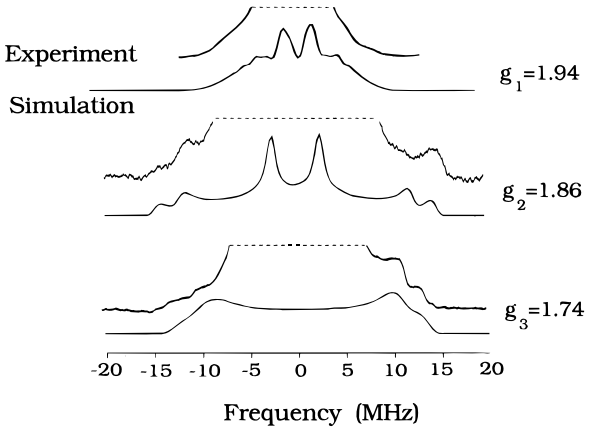

Figure 12. Simulation of the $MMOH_{mv}$ hydroxide bridge proton ENDOR data. Simulations (lower traces) are shown for native $MMOH_{mv}$ proton ENDOR data (upper traces) obtained at three *g*-values. Simulations were performed using the **A** tensor calculated with the geometry of Figure 10 (Appendix I), rotated by 45° about the g_2 axis. The simulations employed an ENDOR line width of 0.5 MHz and EPR line widths, associated with *g* strain, of 100 G. The experimental data are truncated in order to emphasize the broad, strongly coupled hydroxide bridge proton ENDOR resonances.

tensor principal axis frame by a rotation about the g_2 axis by the angle $\theta = 45(5)°$.

The successful prediction of the tensor components confirms the assignment of the ENDOR signals to a hydroxide bridge proton that interacts with the spin-coupled cluster via a sum of through-space, point-dipole interactions within the geometric model of Figure 10. In particular, and somewhat surprisingly, there is no need to invoke substantial local interactions from electron spin delocalized onto the bridging oxygen atom in order to simulate the experimental spectrum.

By comparing the experimentally determined orientation of **A** in the **g** frame with the calculated orientation of **A** in the molecular frame (**e**), these simulations further allow us to infer the orientation of the **g** tensor relative to the molecular **e** frame. As shown in Figure 11, this comparison indicates that g_2 is normal to the Fe(OH)Fe plane (collinear with e_2), and $\gamma \sim \theta \sim 45°$ indicates that either g_3 or g_1 lies along the Fe−Fe direction, e_3. The analysis of the ^{15}N1 ENDOR data indicated that the Fe^{3+}−N1 bond makes a ∼30° angle with g_3; this result, when compared with the structure of diferric $MMOH_{ox}$, slightly favors g_1 as lying along the Fe−Fe direction. The similar field dependence of the ENDOR signals from the hydroxo bridge proton in DMSO-treated $MMOH_{mv}$ indicates that the orientation of **g** is unchanged by DMSO binding.

Nitrogen Hyperfine Couplings. The EPR properties of mixed-valence diiron centers have been extensively characterized for proteins and model compounds,[52,53] but there have been few studies of ligand hyperfine couplings in such centers.[15,21,41,44] The ENDOR data for $MMOH_{mv}$ include resonances for the two histidyl ligand nitrogen nuclei, N1 and N2. From the ^{15}N tensors of Table 2, one can calculate ^{14}N isotropic hyperfine couplings of ∼5.5 and 17 MHz; assigning these values to the ferrous and ferric sites, respectively, these values correspond to "single-ion" isotropic hyperfine values for Fe^{2+} and Fe^{3+}-bound ^{15}N of $a_{iso} \sim +4$ and +7 MHz according to eq 4b. The signs of the hyperfine couplings are not determined but the single-ion parameters are *a priori* expected to be positive. The fraction of unpaired electron spin density in the 2s orbital of each nitrogen nucleus (f_{2s}) is then related to the isotropic hyperfine coupling by eq 5, where $a°(^{14}N) = 1163$ MHz is the hyperfine

Table 4. Spin Hamiltonian Parameters for $MMOH_{mv}$ (*Mc*)[a,b]

	$MMOH_{mv}$			$MMOH_{mv}$ + DMSO		
g(obs)	1.94	1.86	1.74	1.95	1.87	1.82
g(Fe^{2+})	$g_y = 2.052$	$g_x = 2.105$	$g_z = 2.173$	$g_z = 2.04$	$g_x = 2.10$	$g_y = 2.12$
D,[b] E[b] (cm^{-1})		−4.7, −1.3			3.3, 0.7	
D_x,[b] D_y,[b] D_z[b] (cm^{-1})		+0.23, +2.9, −3.1			−0.45, −1.8, +2.2	
A(Fe^{3+})(calc)[c]	63	68	75	65	70	72
A(Fe^{3+})(obs)[d]	62	68	76	62	68	76
a(Fe^{2+})[e]	-27	-32	−3	−33	−28	−7
A(Fe^{2+})(calc)[f]	37	36	5	39	38	11
A(Fe^{2+})(obs)[d]	38	38	n.d.	36	38	<20
t_{2g} ground[g] state		d_{xy}			d_{xz}	

[a] Hyperfine values given in MHz. Analysis procedure is described in the text and in Appendix II (supporting information). [b] Parameters defined as: **g**(Fe^{3+},Fe^{2+}), **a**(Fe^{3+},Fe^{2+}) are single-ion **g** and hyperfine tensors; **A**(Fe^{3+},Fe^{2+}) are cluster hyperfine tensors; $D_{x,y,z}$[b] are Fe^{2+} zero-field splitting tensor elements; $D^b = 3D_z{}^b/2$, $E^b = (D_x{}^b - D_y{}^b)/2$. The intrinsic tensors **g**(Fe^{3+}) and **a**(Fe^{3+}) are assumed to be isotropic with values of 2.0 and −29.5 MHz, respectively; zero-field splitting on Fe^{3+} is assumed to be zero. [c] Calculated using eq A9, adapted from Sage *et al.*[51] [d] From Table 3. [e] Calculated from eq A10. [f] Calculated from eq A12, adapted from Sage *et al.*[51] [g] For high-spin, d^6 ($S = 2$) Fe^{2+} ion.

$$a_{iso} = f_{2s}a^{\circ}_{2s}/2S \qquad (5)$$

coupling for a spin population of unity.[55] For the ferrous site nitrogen, $S = 2$ and $f_{2s} \cong 1.4\%$; for the ferric site nitrogen, $S = {}^5/_2$ and $f_{2s} \cong 3\%$. These values respectively compare quite favorably to those previously reported for the two histidines coordinated to the ferrous ion of the Rieske 2Fe−2S cluster[44] ($f_{2s} \cong 1.5$ and 2%) and to the proximal histidine ligand of the ferric center in metmyoglobin ($f_{2s} \cong 3\%$).[45] Thus, the nature of the additional Fe ligands, S^{2-} for the Rieske center and O-donors for $MMOH_{mv}$, does not appear to have a major influence on spin delocalization to the Fe−N(His) bonds.

Analysis of ^{57}Fe Tensors. The ^{57}Fe hyperfine couplings to both iron ions of a dinuclear center, but especially the ferrous site, are sensitive to the ligand field at the ferrous ion. Thus, major changes in coordination at Fe^{2+} could be expected to lead to appreciable changes in the $A(^{57}Fe)$: such changes are not observed upon DMSO treatment of $MMOH_{mv}$. Table 3 lists the full ^{57}Fe hyperfine tensors for the ferric and ferrous sites of DMSO-treated $MMOH_{mv}$, plus the ferric and two of the three ferrous tensor components for native $MMOH_{mv}$. The values determined from Mössbauer studies of DMSO-treated $MMOH_{mv}$ from *M. trichosporium*, which agree well in magnitude with those reported here, are also listed; tensor orientations are not available from the Mössbauer measurements.[56]

Determination of the tensor orientations is important because theory predicts that the direction of the unique value of the Fe^{2+} hyperfine tensor relative to the cluster **g**-tensor is determined by the lowest-energy ferrous-ion d-orbital, as fixed by the ferrous ion ligand field.[24,36,51−53] Similarly, if the strong-coupling limit of eqs 4 does not hold, the ferric-ion hyperfine tensor becomes anisotropic because of spin-state mixing that arises through the action of the ferrous ion ligand field.[51] The ^{57}Fe hyperfine tensors of $MMOH_{mv}$ were analyzed so as to determine the ferrous-ion ground state and describe its ligand field, using the procedure presented in Appendix II (supporting information). The resulting cluster zero-field splitting parameters and predicted ferrous ion t_{2g} ground states are given for native and DMSO-treated $MMOH_{mv}$ in Table 4; the success of the analysis is evident in the excellent agreement between calculated and observed ^{57}Fe hyperfine tensors for the two Fe ions.

A central experimental result used in the analysis is that for both native and DMSO-treated $MMOH_{mv}$, the unique ferrous-ion ^{57}Fe hyperfine direction is associated with g_3. Because the ground-state t_{2g} orbital lies in the plane perpendicular to this unique hyperfine direction,[24,36] this means that treatment of $MMOH_{mv}$ with DMSO does not change the orientation of the ground-state orbital with respect to **g** or the molecular **e**-frame (Figure 11), a finding that provides further evidence against substantial perturbation at the ferrous ion. Note that this conclusion is not contradicted by the fact that the analysis assigns different ferrous-ion ground states to the native and DMSO-treated enzyme, d_{xy} and d_{xz}, respectively (Table 4). As explained in the supporting information, the changes result merely from the use of a convenient but arbitrary and nonphysical convention for assigning (x, y, z) axes to the Fe^{2+} zero-field splitting tensor. Because $MMOH_{mv}$ has a near-rhombic cluster **g** tensor, in this convention the small changes in g-value upon DMSO treatment lead to a change in the *name* of the ground-state d-orbital without a change in the orbital itself.

Position of Bound DMSO. The above determination of the maximum observed ^{2}H and ^{13}C hyperfine couplings between labeled DMSO with the dinuclear Fe center, $A(^{13}C) \sim 1.3$ MHz and $A(^2H) \sim 1$ MHz, allows us to define the locus of possible positions for the interacting methyl group(s) of DMSO through the use of eqs A1 and A2 (Appendix I). This locus is an ellipsoid of revolution, the axis of which is the Fe−Fe vector, Figure 13; Because of the unequal coupling coefficients in eqs A1 and A2, the surface is asymmetric with respect to the two Fe ions. For locations substantially nearer to Fe^{3+} than to Fe^{2+} (to the right in Figure 13), the acceptable locations of the methyl group can be loosely approximated by the surface of a sphere centered on Fe^{3+} and of radius $\gtrsim$4 Å. For locations substantially nearer to the ferrous ion than to the ferric (to the left in Figure 13), the surface can be approximated by a significantly smaller sphere, with radius of ∼3.2−3.7 Å.

Model (μ-oxo)bis(μ-carboxylato)diiron(III) compounds show that DMSO bound by its oxygen atom to Fe has one methyl at distances no shorter than *ca.* 4 Å from the metal,[57] and the other at no less than *ca.* 4.4 Å. According to Figure 13, a methyl location that yields the observed maximum hyperfine splittings from DMSO and that also has an Fe−C distance of no less than *ca.* 3.8−4 Å requires that the methyl be closer to Fe^{3+} than to Fe^{2+}, the only exception being a band around the waist of the complex where the distances to the two iron ions are

(55) Morton, J. R.; Preston, K. F. *J. Magn. Reson.* **1978**, *30*, 577−582.

(56) Lacking orientational information, the Mössbauer studies of DMSO-treated $MMOH_{mv}$(*Mt*) were interpreted by a model that predicted the smallest value of the ferrous hyperfine tensor to correspond with the largest g-value (g_1) in DMSO-treated $MMOH_{mv}$. This predicted orientation could not be adequately tested by the accompanying X-band ENDOR study (ref 24) and is in disagreement with the tensor orientations determined experimentally here for $MMOH_{mv}$(*Mc*) (Table 3).

(57) Ward, K. L.; Lippard, S. J. To be submitted for publication.

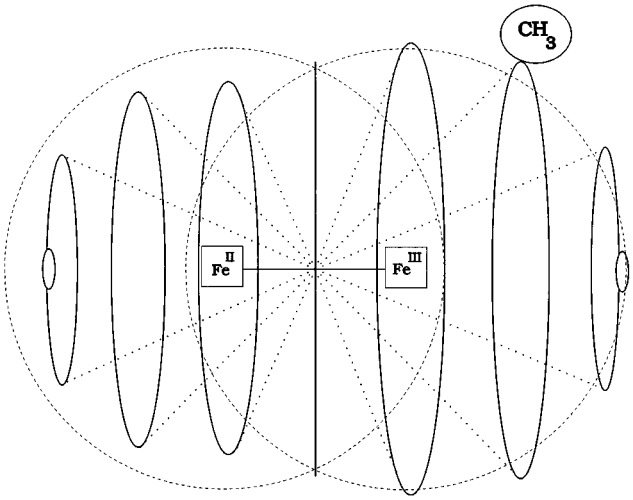

Figure 13. Possible positions of DMSO methyl groups relative to the dinuclear Fe center of $MMOH_{mv}$. The hyperfine parameters of ^{13}C and ^{2}H of labeled DMSO were used, as described in the text, to determine the (approximate) set of possible locations of these nuclei with respect to the Fe nuclei of $MMOH_{mv}$. The edges of the cones represent slices through the ellipsoid of revolution that represents allowed positions, as determined by requiring that the maximum ^{2}H and ^{13}C hyperfine couplings match those observed (Figure 8). The dashed circles about each of the Fe atoms have radii of 4 Å, which is the approximate value expected for a methyl group of DMSO bound to Fe through the oxygen atom.

comparable. The ESEEM data further indicate an unsymmetrical orientation of the DMSO methyl groups, with one methyl appreciably closer to the diiron center as in the model complexes.

In summary, the analysis of the ^{2}H and ^{13}C ENDOR data for labeled DMSO strongly suggests that DMSO binds through its oxygen atom to the ferric ion of $MMOH_{mv}$, in a structure with one methyl group at a distance of ~4 Å from Fe^{3+}. This putative DMSO binding does not cause loss of the aqua ligand from the Fe^{2+} ion. The ^{57}Fe ENDOR analysis supports the assignment of DMSO binding at Fe^{3+} in that the DMSO-induced changes in the ferrous ion parameters in fact reflect only minor perturbations at the environmentally sensitive Fe^{2+} ion. Correspondingly, the $^{14,15}N$ data show appreciably greater perturbation to the ferric ion ligand, N1. The observation of a heterogeneous EPR signal and two populations of the N1 ligand to Fe^{3+} further suggests there may be two discrete, alternate geometries of bound DMSO; and the second reflects a solvent-perturbed form.

Molecular Model for DMSO Binding to $MMOH_{mv}$. It is possible to suggest a molecular model for such DMSO binding to $MMOH_{mv}$ by considering the ENDOR data within the context of the crystal structure information obtained for MMOH (Figure 1). In $MMOH_{ox}$ one of the Fe atoms is six-coordinate, and the other is pseudo six-coordinate, with one of the bridging carboxylate oxygen atoms from Glu 144 forming a relatively long interaction. In $MMOH_{red}$, both iron atoms have an available site. The $MMOH_{mv}$ form of the enzyme that is observed in these ENDOR experiments is not expected to have the bridging acetate shown in Figure 1a, because the buffer used here contains no acetate or other such small molecules that would occupy a bridging position. Thus, in the $MMOH_{mv}$ form, both Fe atoms might be 5-coordinate, as in $MMOH_{red}$, leaving vacancies available on either or both of the Fe atoms for DMSO to occupy as a ligand. Alternatively, one or more of the carboxylate groups from Glu residues that provide monodentate ligation to the Fe atoms in the diferric structure of MMO may shift to bidentate ligation in the absence of acetate, creating one or more six-coordinate Fe atoms in $MMOH_{mv}$. This type of "carboxylate shift" has been proposed as one method by which proteins may maintain a flexible coordination sphere during reaction turnover,[58] as observed when the protein is reduced (Figure 1).

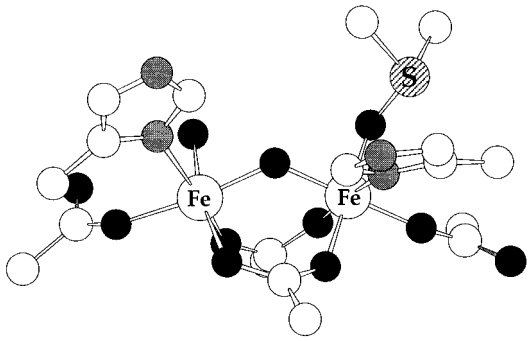

Figure 14. Model of the $MMOH_{mv}$ cluster with DMSO bound to the Fe^{3+} ion. The model was made by using the program CHARMm, as described in the text. Although the DMSO is drawn *cis* to His 246, we do not exclude a *trans* geometry.

Given the above considerations, DMSO might bind either by addition to a 5-coordinate Fe^{3+} ion or by inducing a carboxylate shift; the ^{1}H ENDOR data show that DMSO does not displace Fe^{2+}-bound H_2O. A plausible model for DMSO bound to $MMOH_{mv}$ is shown in Figure 14. In this model, the bridging acetate or water in $MMOH_{ox}$ is replaced by a bridging Glu 243. The oxygen atom of the DMSO ligand is then placed in the site originally occupied by the Glu 243 oxygen donor in the crystal structure (Figure 1). The resulting complex has two octahedrally coordinated iron atoms. The structure so generated was then used as the starting point for a molecular mechanics refinement by using CHARMm,[59] where the geometry was fixed except for the torsion angles about the Fe−O and O−S bonds of the coordinated DMSO molecule. A correlation map of the two $Fe^{3+}\cdots CH_3$ distances, as a function of potential energy, revealed two families of low energy structures, one with values of 3.7 and 4.7 Å, the other with 4.1 and 4.4 Å. A member of the latter family of structures is illustrated in Figure 14, where the DMSO ligand is shown bound to the ferric ion of the dinuclear center and the water molecule to the ferrous ion.

Summary and Conclusions

Results from ENDOR and ESEEM Spectroscopic Studies of Native and DMSO-Treated $MMOH_{mv}$. Key chemical and biochemical results from the spectroscopic studies reported here include the following.

(1) The $^{14,15}N$ and $^{1,2}H$ ENDOR signals from native and DMSO-treated $MMOH_{mv}$ indicate that this exogenous ligand perturbs both histidine ligands to the cluster, but does not displace either of them or the aqua ligand coordinated to Fe^{2+}, nor does it alter the hydroxo bridge. Since the terminal water molecule in both $MMOH_{ox}$ structures and the weakly bound terminal water in $MMOH_{red}$ are all on the same iron atom, we conclude that DMSO binds the other Fe atom. The analysis of ^{13}C and ^{2}H hyperfine couplings to DMSO labeled at the methyl groups is interpreted to indicate that DMSO is O-bonded to Fe^{3+} and serves as the basis for molecular modeling that leads to the structure of the DMSO-bound diiron center shown in Figure 14. Thus it appears that the Fe^{3+} of $MMOH_{mv}$ has either an

(58) Rardin, R. L.; Tolman, W. B.; Lippard, S. J. *New J. Chem.* **1991**, *15*, 417−430.
(59) Swaminathan, S.; Karplus, M. J. *J. Comput. Chem.* **1983**, *4*, 187−217.

open coordination site or an easily substituted site at which DMSO can bind, whereas the Fe^{2+} site aqua ligand appears to be less susceptible to substitution by DMSO. A reasonable scenario in which DMSO binds at the site where O_2 binds to the cluster would explain the ability of DMSO to inhibit methane oxidation. The aqua ligand may serve then as a second labile site, or a source of protons, utilized later in the catalytic scheme.

(2) ENDOR signals from the proton of the $MMOH_{mv}$ hydroxide bridge could be analyzed in terms of a point-dipole model for the spin-coupled dinuclear Fe center, which implies that spin delocalization to the bridging O atom is minimal. Further, a surprisingly symmetric orientation of the molecular **g**-tensor, with one unique component along the Fe−Fe direction, was inferred from the parameters required to simulate the proton data and was not changed by the binding of DMSO. This supports the conclusion that DMSO binds to Fe^{3+}, for the **g**-tensor orientation is largely determined by the bonding to Fe^{2+}.

(3) Finally, ^{57}Fe hyperfine tensors including the orientations as well as the components have been determined for both Fe^{2+} and Fe^{3+} sites of the dinuclear center and both ^{57}Fe hyperfine tensors have been successfully analyzed in terms of the ligand-field splitting at Fe^{2+} (Table 4; Appendix I, supporting information). An analysis of the Fe^{2+} local **g**-tensor in combination with the measured orientation of the Fe^{2+} hyperfine tensor shows minimal changes in ligand field, in particular that the orientation of the ground state t_{2g} orbital of the d^6 ferrous ion does not change with respect to the molecular framework upon treatment of $MMOH_{mv}$ with DMSO.

Application of Advanced Magnetic Resonance Techniques to $MMOH_{mv}$. This study also serves as a reference for the use of advanced paramagnetic resonance techniques in the study of carboxylate-bridged diiron centers.[19,20] We found that continuous wave Q-band ENDOR spectroscopy gave excellent results for the relatively broad ENDOR (nmr) lines of $^{14,15}N$, ^{1}H, and ^{57}Fe coupled to the $MMOH_{mv}$ dinuclear Fe center. The absorptive line shapes (see Methods) given by the CW detection scheme employed are particularly useful in the case of broad and low-amplitude signals, such as those for the hydroxide bridge proton. The higher frequency of Q-band (35 GHz), as opposed to the conventional X-band frequency (9 GHz), is necessary to resolve signals from protons and heteronuclei; for example, at X-band one would observe significant overlap between the ^{1}H spectra (centered at ∼14 MHz and with a width of >10 MHz) and ferrous-site ^{57}Fe resonances (centered at ∼18 MHz), or ^{15}N (N1 centered at ∼12 MHz).

For weakly-coupled nuclei, such as the ^{13}C and ^{2}H of DMSO, pulsed or "echo-detected" ENDOR techniques are superior to the CW method.[30] For $MMOH_{mv}$, detection of ENDOR by monitoring the electron spin echo is technically difficult because the electron-spin system dephases quickly, yet has relatively long T_{1e}'s.[22] The former causes a dramatic reduction (∼80%) in the intensity of the electron spin−echo intensity as detected at the end of the ENDOR pulse sequence; the latter severely limits the data-acquisition rate. These difficulties were overcome because of the enhanced signal-to-noise ratio of a new Q-band pulsed ENDOR spectrometer.[32] The increase in frequency from X- to Q-bands also moves the ^{2}H and ^{13}C resonances to a higher radio frequency range, where the ENDOR response is bigger. Finally, X-band ^{2}H ESEEM spectroscopy was used to give information about the numbers of nuclei involved in a resonance. This knowledge complements the ENDOR data, with the net result being detailed structural information about the binding of labeled DMSO to the $MMOH_{mv}$ center. Only the combined use of all of these techniques made possible the broad range of structural and electronic information reported here for the dinuclear Fe center of $MMOH_{mv}$. This same strategy will be used to study the binding of protein B and of methanol to MMOH.

Acknowledgment. This work relied on the technical expertise of Mr. C. E. Davoust and was supported by the NIH (GM 32134 (S.J.L.), HL 13531 (B.M.H.), Predoctoral Trainee CA 09112 (K.E.L.), Postdoctoral GM 14259 (V.J.D.)) and the NSF (MCB 9207974 (B.M.H.)). The Q-band pulsed spectrometer was purchased with a grant from the NIH (DRR-04936). We thank Dr. S. U. Dunham for assistance with the molecular mechanics calculations.

Appendix I. Calculation of Angle-Dependent ENDOR Frequencies for the Proton of a Hydroxide Bridge

One can calculate the hydroxo bridge proton ENDOR frequencies for a particular molecular orientation with respect to the external magnetic field with eq A1, where the contributions from the two Fe ions have the classical form for point-dipole interaction (eq A2). In eq A2, r_{iH} refers to the distance between the proton and the ferric (i = a) or ferrous (i = b) ion,

$$\nu_{\pm} = \nu_H \pm \frac{A}{2}; \qquad A = {}^{7}/_{3}a^{q}_{dip} - {}^{4}/_{3}a^{b}_{dip} \tag{A1}$$

$$a^{i}_{dip} = \frac{g_e g_N \beta_e \beta_n}{h}\left[\frac{1}{r^3_{iH}}(3\cos^2\varphi_i - 1)\right] \tag{A2}$$

and φ_i refers to the angle between the external magnetic field and the vector connecting the proton and the ith iron ion. In the symmetrical model of Figure 10, $r_{aH} = r_{bH} \equiv r_{Fe-H}$ and ϕ_a and ϕ_b can be readily calculated for any magnetic field orientation.

In early phases of this work the general behavior of this point-dipolar model was investigated by exploring the orientation dependence of eq A1; similar calculations have been presented by others.[60] These calculations demonstrated that the model correctly predicted highly anisotropic interactions with the maximum coupling of $A \sim 30$ MHz, as seen in Figure 4. The locus of points in Figure 13 was derived by calculating the maximum possible value of dipolar hyperfine coupling for a given position of a methyl group, through systematic sampling of all possible orientations of the molecule in a static external magnetic field.

Detailed simulations of the orientation-selective spectra collected at various fields within the EPR envelope (e.g., Figures 4 and 12) are based on the effective spin Hamiltonian, however, and are better formulated in terms of the cluster hyperfine tensor of the spin-coupled system (**A**; eq A6). We therefore considered a nucleus at an arbitrary location, took the dipolar tensors for its interactions with the individual uncoupled iron ions, ($\mathbf{a}^a$ and $\mathbf{a}^b$, eq A2), expressed them in a common axis frame of Figure 10, added them according to eq A1, and diagonalized the resultant to obtain the effective hyperfine tensor **A** for the $S = {}^{1}/_{2}$ ground state Hamiltonian of the spin-coupled cluster system (to be published). For the particular case of the hydroxide bridge proton, we chose to parametrize **A** for a given geometry of Fe(OH)Fe in terms of r_{Fe-H} and the angle β that is subtended by the Fe^{III}−H and Fe−Fe vectors (Figure 10). Within the structural model of Figure 10 the dipolar interaction tensor A

(60) Khangulov, S.; Sivaraja, M.; Barynin, V. V.; Dismukes, G. C. *Biochemistry* **1993**, *32*, 4912−4924.

(eqs A1 and A2) has principal values given in eqs A3a and A3b.

$$\mathbf{A} \equiv [A_1, A_2, A_3] \equiv T[\alpha_1, \alpha_2, \alpha_3] \tag{A3a}$$

$$T = \frac{g_e\beta_e g_n\beta_n}{r^3_{Fe-H}};$$

$$\alpha_1 = \frac{1}{4}\left[1 - 11\frac{\sin 2\beta}{\sin 2\gamma}\right], \quad \alpha_2 = -1/2, \quad \alpha_3 = \frac{1}{4}\left[1 + 11\frac{\sin 2\beta}{\sin 2\gamma}\right];$$

$$\tan 2\gamma = {}^{11}/_{3} \tan 2\beta \tag{A3b}$$

The hyperfine frame is related to the molecular [e_1, e_2, e_3] frame by a rotation around e_2 through the angle γ.

With the metrical parameters of Figure 10, $r_{Fe-H} = 2.5$ and $\beta = 51°$, the predicted dipolar tensor components are given in eq A4 and the orientation of the tensor relative to the molecular frame is illustrated in Figure 11.

$$\mathbf{A} = [-25, -5, +30] \text{ MHz}$$
$$\gamma = 47° \tag{A4}$$

Supporting Information Available: Appendix II, analysis procedures and figures showing the orientation dependence of υ_+ (^{15}N1) resonances from DMSO-treated $MMOH_{mv}$ and ^{57}Fe ENDOR of the ferric and ferous sites in $MMOH_{mv}$ (10 pages). This material is contained in libraries on microfiche, immediately follows this article in the microfilm version of the journal, can be ordered from the ACS, and can be downloaded from the Internet; see any current masthead page for ordering information and Internet access instructions.

JA951108V